Int. J. Heat Mass Transfer. Vol. 31, No. 5, pp. 941–955, 1988
Printed in Great Britain

0017–9310/88 $3.00 + 0.00

Natural convection boundary layer flows in isothermal ternary systems: role of diffusive coupling

ALAIN F. TRIAL and FRANK J. SPERA
Department of Geological Sciences, University of California, Santa Barbara, CA 93106, U.S.A.

(*Received* 4 *February* 1987 *and in final form* 9 *September* 1987)

Abstract—The effects of diffusive cross-coupling on an isothermal natural convection boundary layer in a large *Sc* fluid has been studied. Results show that the off-diagonal diffusion coefficient is important when the appropriate ratio, β_{12}/β_{22} or β_{21}/β_{22}, is larger than approximately 10^{-1}. Uphill diffusion and accompanying compositional extrema may result when $\beta_{12} > \beta_{22}$ or $\beta_{12} < 0$ for component 1 and when $\beta_{21} > 1$ or $\beta_{21} < 0$ for component 2. Counterflow may result when $\beta_{21} < 0$ or $\beta_{12} < 0$ even for positive buoyancy ratios. Effective binary diffusion coefficients are inadequate for representing multicomponent systems with large off-diagonal diffusion coefficients. Published determinations of the full diffusion matrix for several multicomponent systems imply that neglect of off-diagonal contributions to the chemical flux may lead to large errors in mass transfer rates in multicomponent systems of geochemical and industrial importance.

INTRODUCTION

NATURAL convection boundary layer flows have been extensively studied over the years. Flows with a single buoyancy source, either thermal [1–6] or compositional [2, 7, 8], have attracted the most attention. Flows with two sources of buoyancy, in particular combined heat and mass transfer [9–13], have been studied less thoroughly. Diffusive cross-coupling is an intriguing aspect of such flows that has been inadequately considered. An exception is the study by Sparrow *et al.* [13] of free convection from a horizontal cylinder in a helium–air mixture. Their numerical results showed that the Soret effect was negligible. but that the Dufour effect significantly altered heat transfer as the mass transfer increased. Similar analyses for incompressible fluids have not been made.

Phenomenological coupling analogous to the Soret and Dufour effects also occurs in isothermal, multicomponent fluids. Measurements of the diffusivity matrix for ternary systems are available for some gases and liquids [14–17]. Table 1 lists diffusivities for the slag systems $CaO–Al_2O_3–SiO_2$ and $K_2O–SrO–SiO_2$ and a seawater analogue, $NaCl–MgCl_2–H_2O$. Note that one or both off-diagonal diffusion coefficients, D_{12} and D_{21}, are large compared to the on-diagonal diffusion coefficients, D_{11} and D_{22}. This is by no means uncommon, judging by the data cited above.

Our interest is in natural silicate liquids (magma). In recent years several geologists have proposed that boundary layer flows play a key role in the chemical evolution of crustal magma chambers [18, 19]. These authors, by necessity, utilize the formalism of effective binary diffusion theory to treat mass transfer along subvertical walls in magma chambers filled with complex, multicomponent magma. It is important to note, however, that laboratory studies on metal oxide–silica multicomponent melts and aqueous multicomponent systems show that diffusive cross-coupling can be extremely important. In fact, in some systems off-diagonal contributions to the flux of a given species may be larger than corresponding on-diagonal terms (see $CaO–Al_2O_3–SiO_2$ in Table 1). Any conclusions regarding rates of mass transfer in magma chambers based on the effective binary approach must remain tentative until either laboratory studies or molecular dynamics simulations [20] provide sufficient information on the complete diffusion matrix for an *n*-component silicate melt of natural composition. Earlier studies [19] of the role of convecto-diffusive sidewall boundary layers in magma chambers may be seriously in error due to an inadequate account of diffusive cross-coupling.

This study quantifies the effects of diffusive cross-coupling on natural convection boundary layer flows in an incompressible fluid with two buoyancy sources. The equations are formulated for an isothermal, ternary system with phenomenological representations for the chemical fluxes. Our analysis exploits the fact that many fluids, including slags, aqueous solutions and liquid metals, have large Schmidt numbers. In addition we present results for which the fluid viscosity is also a function of composition. This latter case is important in geochemical and geothermal applications [21, 22]. We will also show that effective binary diffusion coefficients (EBDCs) are inadequate for representing multicomponent systems with large off-diagonal diffusion coefficients. Elsewhere we will apply the results of this study to SiO_2 and H_2O transport in crustal magma chambers.

NOMENCLATURE

A_{ij}	coefficient of variation for D_i with ω_j, equations (A1)
B_i	coefficient of variation for viscosity with ω_i, equation (2)
D_i	effective binary diffusion coefficient, equations (A1)
D_{ij}	phenomenological diffusivity matrix
f	stream function in similarity variable space, equation (9b)
Gr_L	length Grashof number, $g\alpha_1\Delta\bar{\omega}_1 L^3/\nu_\infty^2$
g	acceleration of gravity
h	characteristic length, $(4\nu_\infty^2/g\alpha_1\Delta\bar{\omega}_1)^{1/3}$
j	non-dimensional mass flux, $j_i[\rho^3 g\alpha_1 D_{11}^3\Delta\bar{\omega}_1\Delta\bar{\omega}_i^3/4\nu_\infty^2]^{-1/3}$
L	height of plate
Sc	Schmidt number, ν_∞/D_{11}
Sh_i	Sherwood number for ith component, equations (10), (11), and (A5)
u	non-dimensional streamwise velocity, $\bar{u}h/\nu_\infty$
v	non-dimensional transverse velocity, $\bar{v}h/\nu_\infty$
x	non-dimensional streamwise coordinate, $\bar{x}/h$
y	non-dimensional transverse coordinate, $\bar{y}/h$.

Greek symbols

α_i	coefficient of compositional expansivity, $-(1/\rho)(\partial\rho/\partial\bar{\omega}_i)$
β_{ij}	non-dimensional phenomenological diffusivity matrix, $(D_{ij}\Delta\bar{\omega}_j/D_{11}\Delta\bar{\omega}_i)$
γ_i	concentration in similarity variable space, equations (9c) and (9d)
Γ	buoyancy rate, $\alpha_2\Delta\bar{\omega}_2/\alpha_1\Delta\bar{\omega}_1$
δ_i	boundary layer thickness for ith component
η	spatial coordinate in similarity variable space, equation (9a)
ν	kinematic viscosity
ρ	density
ψ	stream function
ω_i	non-dimensional weight fraction of ith component, $(\bar{\omega}_i-\bar{\omega}_{i\infty})/\Delta\bar{\omega}_i$
$\Delta\bar{\omega}_i$	concentration difference across the boundary layer, $(\bar{\omega}_{iw}-\bar{\omega}_{i\infty})$.

Subscripts and superscripts

i,j	refer to the ith or jth chemical component
w	value of a quantity at the plate surface, $y=0$
∞	value of a quantity in the fluid bulk
$\bar{}$	overbar denotes dimensional quantities.

Table 1. Phenomenological diffusion coefficients (D_{ij} have units of $m^2\,s^{-1}$)

System	D_{11}	D_{12}	D_{21}	D_{22}	Ref.
40 wt % CaO (1)† 20 wt % Al_2O_3 (2) 40 wt % SiO_2 (3)	10^{-10}	-2.8×10^{-11}	-4.2×10^{-11}	7.3×10^{-11}	[15]
21.5 wt % K_2O (1)‡ 18.0 wt % SrO (2) 60.5 wt % SiO_2 (3)	9.25×10^{-14}	1.72×10^{-15}	-1.1×10^{-13}	10^{-17}	[16]
0.489 M NaCl (1)§ 0.051 M $MgCl_2$ (2) H_2O (3)	1.4×10^{-9}	7.1×10^{-10}	2.6×10^{-11}	7.4×10^{-10}	[17]

† $T = 1500$°C.
‡ $T = 806$°C.
§ $T = 25$°C.

MATHEMATICAL DEVELOPMENT

Consider a flat vertical plate bounding a large body of incompressible, isothermal fluid. The x-coordinate axis is vertical and extends upwards from the leading edge while the y-coordinate axis is perpendicular to the plate and is measured from the surface of the plate. Velocities u and v are parallel to the x- and y-axes, respectively. At the plate, two solute species are maintained at the constant weight fractions $\bar{\omega}_{1w}$ and $\bar{\omega}_{2w}$ which are greater than their weight fractions in the bulk fluid, $\bar{\omega}_{1\infty}$ and $\bar{\omega}_{2\infty}$. Following the usual practice in free convection, the fluid density is considered constant except in deriving the buoyancy terms. For this buoyancy force we assume fluid density is a linear function of composition as given by

$$\rho = \rho_\infty[1-\alpha_1(\bar{\omega}_1-\bar{\omega}_{1\infty})-\alpha_2(\bar{\omega}_2-\bar{\omega}_{2\infty})]. \quad (1)$$

Compositional expansivities are given in Table 2 for the three systems listed in Table 1 and for magmas. Since density measurements are not readily available for the slag systems and magmas, we have estimated α_i using densities calculated by the method of ref. [23].

Table 2. Density function (ρ is in kg m^{-3})

System		α_1	α_2	ρ	Ref.
40 wt % CaO	(1)†				
20 wt % Al_2O_3	(2)	-0.28	7.5×10^{-4}	2681	
40 wt % SiO_2	(3)				
21.5 wt % K_2O	(1)‡				
18.0 wt % SrO	(2)	-0.036	-0.61	2562	
60.5 wt % SiO_2	(3)				
0.489 M NaCl	(1)§				
0.051 M $MgCl_2$	(2)	-6.82×10^{-4}	-8.04×10^{-4}	1020.78	[17]
H_2O	(3)				
Basaltic magma:					
H_2	(1)	2.0	0.3	2278	[32]
SiO_2	(2)				

† $T = 1500$°C.
‡ $T = 806$°C.
§ $T = 25$°C.

As long as $\Delta\bar{\omega}_i$ is sufficiently small that $\alpha_i\Delta\bar{\omega}_i \ll 1$ the linear approximation is valid. We further require α_1 and α_2 have the same sign although, significantly, we will show this is *not* a sufficient condition for avoiding opposed buoyancy effects.

Since silicate liquids have strongly composition-dependent viscosities, the kinematic viscosity is made a function of composition

$$\nu = \nu_\infty \exp\left[B_1\omega_1 + B_2\omega_2\right]. \tag{2}$$

This exponential viscosity law adequately describes the behavior of silicate liquids over a wide composition range [22, 24].

Using the boundary layer approximation, conservation of mass and momentum are given by equations (3) and (4) in non-dimensional form. Note that the length scale has been chosen so that, without loss of generality, a Grashof number does not appear in the momentum equation

$$\frac{\partial u}{\partial x} + \frac{\partial v}{\partial y} = 0 \tag{3}$$

$$u\frac{\partial u}{\partial x} + v\frac{\partial u}{\partial y} = (\omega_1 + \Gamma\omega_2) + \exp\left[B_1\omega_1 + B_2\omega_2\right] \times \left\{\frac{\partial^2 u}{\partial y^2} + B_1\frac{\partial u}{\partial y}\frac{\partial \omega_1}{\partial y} + B_2\frac{\partial u}{\partial y}\frac{\partial \omega_2}{\partial y}\right\}. \tag{4}$$

In order to write conservation equations for the two chemical components, we use the generalization of Fick's law to a ternary system

$$j_1 = -(\nabla\omega_1 + \beta_{12}\nabla\omega_2) \tag{5a}$$

$$j_2 = -(\beta_{21}\nabla\omega_1 + \beta_{22}\nabla\omega_2) \tag{5b}$$

where the solute species are numbered so that $D_{11} \geqslant D_{22}$. We assume that the diffusivities are not composition dependent. Although Gupta and Cooper [25] have shown that this cannot be true in general it seems to be a reasonable approximation as long as composition variations are small. Over the compositional range of the experimental diffusion couples, the measured diffusivities in Table 1 are essentially constant, for example. In order that the inter-diffusivity matrix has real positive eigenvalues [16], the following conditions must be satisfied:

$$|\beta_{22}| \leqslant 1 \tag{6a}$$

$$\beta_{22} \geqslant \beta_{12}\beta_{21} \tag{6b}$$

$$(1+\beta_{22})^2 \geqslant 4(\beta_{22} - \beta_{12}\beta_{21}). \tag{6c}$$

Allowable combinations of the β_{ij} lie within the shaded region of Fig. 1.

We also consider the pseudo-binary approach for representing the fluxes. This only requires two EBDCs which we have made functions of composition. Development of conservation equations for pseudo-binary and full ternary formulations are similar so only the latter will be presented below. The appendix contains corresponding equations for composition-dependent EBDC.

With these expressions for the fluxes, the conservation equations for solute species 1 and 2 are

$$u\frac{\partial \omega_1}{\partial x} + v\frac{\partial \omega_1}{\partial y} = \frac{1}{Sc}\left[\frac{\partial^2 \omega_1}{\partial y^2} + \beta_{12}\frac{\partial^2 \omega_2}{\partial y^2}\right] \tag{7a}$$

$$u\frac{\partial \omega_2}{\partial x} + v\frac{\partial \omega_2}{\partial y} = \frac{1}{Sc}\left[\beta_{21}\frac{\partial^2 \omega_1}{\partial y^2} + \beta_{22}\frac{\partial^2 \omega_2}{\partial y^2}\right]. \tag{7b}$$

The usual velocity boundary conditions for free convection are no slip at the wall and zero velocity in the ambient medium far from the wall. If $\bar{\omega}_{1w}$ amd $\bar{\omega}_{2w}$ are maintained by injecting the solute at the wall, the normal velocity will not be zero; however, when the mass transfer rate is small and the concentrations are low, the normal velocity will also be small [26]. Therefore, relevant boundary conditions are

$$\begin{aligned}(\omega_1 - 1) = (\omega_2 - 1) = u = v = 0 \quad &\text{at } y = 0\\ \omega_1 = \omega_2 = u = 0 \quad &\text{at } y = \infty.\end{aligned} \tag{8}$$

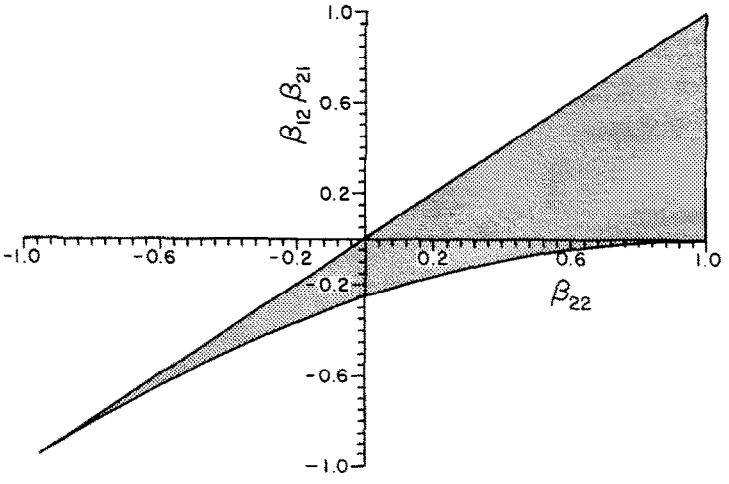

FIG. 1. The thermodynamic constraints in equations (6) require that β_{12}, β_{21} and β_{22} lie in the shaded area of this graph.

Equations (3), (4), (7) and (8) can be reduced to ordinary differential equations by use of the similarity variable method. For a large Schmidt number fluid, the problem can be divided into an inner compositional boundary layer and an outer velocity boundary layer by introducing a stretching transformation [3–5, 8, 12]. The outer problem need be solved only once since fluid in the velocity boundary layer is isocompositional. The outer solution and matching procedure is presented elsewhere [5, 8]. The stretching transformation eliminates advection terms in the momentum equation for the inner compositional boundary layer. Additionally, the condition that shear stress vanishes at the edge of the compositional boundary layer replaces the zero velocity condition in conditions (8).

Introducing stretched similarity variables

$$\eta = (3Sc)^{1/4} y x^{-1/4} \tag{9a}$$

$$f(\eta) = 1/4(3Sc)^{3/4} x^{-3/4} \psi \tag{9b}$$

$$\gamma_1(\eta) = \omega_1 \tag{9c}$$

$$\gamma_2(\eta) = \omega_2 \tag{9d}$$

and taking the limit as Sc tends to infinity leads to the following set of ordinary differential equations where primes denote differentiation with respect to η:

$$f''' + (B_1\gamma_1' + B_1\gamma_2')f'' + \exp[-(B_1\gamma_1 + B_2\gamma_2)](\gamma_1' + \Gamma\gamma_2') = 0 \tag{4'}$$

$$\gamma_1'' + \beta_{12}\gamma_2'' + f\gamma_1' = 0 \tag{7a'}$$

$$\beta_{21}\gamma_1'' + \beta_{22}\gamma_2'' + f\gamma_2' = 0 \tag{7b'}$$

$$f(0) = f'(0) = \gamma_1(0) - 1 = \gamma_2(0) - 1 = f''(\infty) = \gamma_1(\infty) = \gamma_2(\infty) = 0. \tag{8'}$$

The mass flux at the wall is a particularly important quantity which can be calculated by evaluating equations (5) at $y = 0$ and integrating over the plate surface. Sherwood numbers are obtained by dividing this mass flux by an equivalent diffusive flux in the absence of advection and multicomponent effects, equations (10a) and (10b). Notice that reference diffusivities for components 1 and 2 are their corresponding on-diagonal diffusivities

$$Sh_1 = \frac{1}{\rho D_{11} \Delta\bar{\omega}_1} \int_0^L \bar{j}_{1w}\, d\bar{x} \tag{10a}$$

$$Sh_2 = \frac{1}{\rho D_{22} \Delta\bar{\omega}_2} \int_0^L \bar{j}_{2w}\, d\bar{x}. \tag{10b}$$

Integrating the mass fluxes leads to the following expressions for Sh_i in terms of stretched similarity variables:

$$Sh_1 = -1.2408(Gr_L Sc)^{1/4}[\gamma_1'(0) + \beta_{12}\gamma_2'(0)] \tag{11a}$$

$$Sh_2 = -1.2408(Gr_L Sc)^{1/4}\left[\frac{\beta_{21}}{\beta_{22}}\gamma_1'(0) + \gamma_2'(0)\right]. \tag{11b}$$

RESULTS

Equations (4'), (7'), and (8') contain six dimensionless parameters: B_1, B_2, β_{12}, β_{21}, β_{22}, and Γ. Table 3 lists values of these parameters for the systems in Table 1. Chosen compositions approximately correspond to the diffusion couples used to measure the diffusivity matrix. The on-diagonal diffusion coefficients are both positive for all systems for which data are available therefore we only consider $\beta_{22} > 0$. Also we consider a very restricted range of viscosity parameters appropriate to silicate liquids. This part of the study involved approximately 200 numerical solutions.

Equations (4'), (A4) and (8') for EBDCs contain

Table 3. Dimensionless parameters

System		$\Delta\bar{\omega}_1$	$\Delta\bar{\omega}_2$	Γ	β_{12}	β_{21}	β_{22}
40 wt % CaO	(1)†						
20 wt % Al_2O_3	(2)	0.08	0.02	-6.7×10^{-4}	−0.07	−1.68	0.73
40 wt % SiO_2	(3)						
21.5 wt % K_2O	(1)‡						
18.0 wt % SrO	(2)	0.0025	0.025	170	0.19	−0.11	10^{-4}
60.5 wt % SiO_2	(3)						
0.489 M NaCl	(1)§						
0.051 M $MgCl_2$	(2)	0.003	0.002	0.78	0.33	0.03	0.52
H_2O	(3)						
Basaltic magma:							
H_2O	(1)	0.03	0.15	0.75	—	—	—
SiO_2	(2)						

† $T = 1500$°C.
‡ $T = 806$°C.
§ $T = 25$°C.

eight dimensionless parameters: B_1, B_2, A_{11}, A_{12}, A_{21}, A_{22}, and Γ. We have considered a very limited range of these parameters (approximately 60 numerical solutions) for the purpose of our comparison.

We present our results in four sections. The first section reviews work on the uncoupled equations. The second section details the effects of diffusive cross-coupling on an isoviscous fluid ($B_1 = B_2 = 0$). The third section presents results for two particular sets of non-zero viscosity parameters ($B_1 = -2$, $B_2 = 3$ and $B_1 = -5.5$, $B_2 = 3.7$). These particular values were chosen because of relevance to boundary layer flows in basaltic and silicic magma chambers, respectively, where component 1 is H_2O and component 2 is SiO_2 [27]. The fourth section deals with effective binary diffusion coefficients. Results are presented in terms of the mass transfer at the plate (Sh_1 and Sh_2); velocity and composition profiles; and boundary layer thicknesses (δ_i is the distance from the plate such that for all $\eta > \delta_i$, $\gamma_i < 0.01$).

Uncoupled equations

This system of equations is obtained from equations (4′), (7′), and (8′) by setting $B_1 = B_2 = \beta_{12} = \beta_{21} = 0$, which leaves only two dimensionless parameters, β_{22} and Γ. Some analytic and numerical results are available [2, 9, 11], but these cover only a limited part of the β_{22}–Γ parameter space. Numerical solutions obtained during the course of this investigation span $10^{-6} \leqslant \beta_{22} \leqslant 1$ at $\Gamma = 0.375$, 0.75 and $0 \leqslant \Gamma \leqslant 100$ for $\beta_{22} = 10^{-1}$.

First we examine the effect of Γ on concentration and velocity fields ($\beta_{22} = 10^{-1}$). As $\Gamma \to 0$ the ternary system behaves dynamically like a binary system because the momentum equation is decoupled from the conservation equation for component 2. In this limit $f'(\infty)$, Sh_1 and Sh_2 are smallest while δ_1 and δ_2 are both at a maximum (Table 4). As Γ increases, $f'(\infty)$ and the mass flux of both components increases while the boundary layers become thinner. In addition, since component 1 contributes little to the buoyancy forces for large Γ, the maximum velocity occurs near δ_2.

Table 4. Solutions for the uncoupled equations for a range of Γ

				Sh_1	Sh_2
Γ	$f'(\infty)$	δ_1	δ_2	$[Gr_L Sc]^{1/4}$	$[Gr_L Sc]^{1/4}$
0.0	0.882	3.22	1.29	0.670	1.580
0.375	0.902	3.17	1.25	0.686	1.630
0.75	0.920	3.12	1.22	0.700	1.674
1.0	0.933	3.09	1.21	0.709	1.702
10.0	1.268	2.52	0.93	0.904	2.280
100.0	2.945	1.59	0.56	1.465	3.802

$B_1 = B_2 = \beta_{12} = \beta_{21} = 0$; $\beta_{22} = 0.1$.

In a similar way β_{22} affects the boundary layers. When this parameter is unity $\gamma_1 = \gamma_2$. As β_{22} decreases, δ_2 decreases exponentially, approaching zero. In this limit, $\gamma_2 = 0$ almost everywhere in the boundary layer and the ternary system again behaves like a binary system. Consequently, δ_1 increases slightly and $f'(\infty)$ decreases to the corresponding binary system values. Compare values of δ_1 and

Table 5. Solution of the uncoupled equations for a range of β_{22}

β_{22}	δ_1	δ_2	$f'(\infty)$	m
1.0	2.80	2.80	1.17	—
0.9	2.83	2.70	1.14	0.384
0.4	2.96	2.02	1.01	0.381
0.2	3.04	1.57	0.948	0.378
0.1	3.12	1.22	0.920	0.374
10^{-2}	3.20	0.55	0.888	0.363
10^{-3}	3.22	0.25	0.883	0.355
10^{-4}	3.22	0.116	0.883	0.350
10^{-5}	3.22	0.053	0.883	0.347
10^{-6}	3.22	0.025	0.883	0.345
0				0.333

m is the exponent in equation (15). $B_1 = B_2 = \beta_{12} = \beta_{21} = 0$; $\Gamma = 0.75$.

$f'(\infty)$ for the cases $\Gamma = 0$ in Table 4 and $\beta_{22} = 10^{-6}$ in Table 5.

If the two components diffuse equally fast, $\beta_{22} = 1$, then the compositional profiles are identical and the Sherwood numbers [11] are given by

$$Sh_1 = Sh_2 = 0.670(Gr_L Sc)^{1/4}(1+\Gamma)^{1/4}. \quad (12)$$

Based on solutions in the range $\beta_{22} > 0.5$ and $0.5 < \Gamma < 2$, Mathers *et al.* [9] suggested the correlations

$$Sh_1 = 0.670(Gr_L Sc)^{1/4}(1+\Gamma\sqrt{\beta_{22}})^{1/4} \quad (13)$$

$$Sh_2 = 0.670(Gr_L Sc)^{1/4}(1+\Gamma\sqrt{\beta_{22}})^{1/4}\beta_{22}^{-3/8}. \quad (14)$$

Our data support this correlation for Sh_1 but show that the correlation for Sh_2 is inappropriate when $\beta_{22} < 0.1$. A more accurate correlation for Sh_2 is

$$Sh_2 = 0.670(Gr_L Sc)^{1/4}(1+\Gamma\sqrt{\beta_{22}})^{1/4}\beta_{22}^{-m} \quad (15)$$

where m is a function of β_{22} (Table 5). In the limit of $\beta_{22} \ll 1$, m approaches 1/3 [11].

Diffusive cross-coupling

For several reasons it is useful to consider the limiting cases of a single non-zero cross-coupling term, i.e. $\beta_{12} = 0$ or $\beta_{21} = 0$. First, these special cases allow us the greatest freedom in choosing parameters. From Fig. 1 it is clear that all combinations of a positive β_{22} and the non-zero cross term meet the thermodynamic constraints. Second, certain physical situations place these kinds of constraints on the diffusivity matrix. At the boundaries of the composition space one or both off-diagonal terms may vanish: $\beta_{12} = 0$ when $\bar{\omega}_1 = 0$ and $\beta_{21} = 0$ when $\bar{\omega}_2 = 0$ [25]. Since the $\Delta\bar{\omega}_i$ appear in the definition of β_{ij}, one of the cross terms will be nearly zero when the concentration difference of a component is small. Third, these results provide the framework for interpreting solutions in which both cross-coupling terms are nonzero.

A single off-diagonal diffusion coefficient only causes significant changes in one boundary layer since the conservation equation changes for only one species. The other conservation equation (for components 1 and 2, respectively, when $\beta_{12} = 0$ or $\beta_{21} = 0$) remains in a pseudo-binary form. The species the conservation equation of which remains pseudo-binary is unaffected by cross-coupling in one very important respect. The compositional profile of this component retains the same shape no matter how large the cross-coupling.

First we set $\beta_{12} = 0$ in order to examine the response of the flow to β_{21}. From the γ_2 profiles presented in Fig. 2, one can immediately see that diffusive cross-coupling adds a new dimension to the boundary layer equations. The solution of the uncoupled equations ($\beta_{21} = 0$) is a concave up curve with a maximum at $\eta = 0$ and a minimum at $\eta = \delta_2$. When $\beta_{21} = 1$ the γ_2 profile develops an inflection point yet the extrema remain at the edges of the boundary layer. The profiles for $\beta_{21} = -1$ and 2, moreover, have an extremum inside the boundary layer. It is well known from diffusion couple experiments [15, 16] that such extrema can also develop in the absence of convection.

Uphill diffusion, the flux of a component up its concentration gradient, is the physical mechanism behind these concentration profiles. If uphill diffusion were impossible, a compositional maximum or minimum could not exist inside the flow for such an extremum would be a plane of no flux separating regions of opposing mass transport. The mass flux would be directed away from a maximum or toward a minimum, neither of which are physically meaningful.

The condition for uphill diffusion of component 2 is

$$j_2\gamma'_2 = -(\beta_{21}\gamma'_1 + \beta_{22}\gamma'_2)\gamma'_2 > 0.$$

Note that β_{21} must be nonzero for this condition to be satisfied. If β_{22} were negative, thermodynamic constraints would require both β_{12} and β_{21} to be nonzero (Fig. 1). In the case of a compositional maximum (e.g. the curve in Fig. 2(a) for $\beta_{21} = 2$), both the mass flux and compositional gradient are positive at the plate. Our work shows that β_{21} must be larger than unity in order for a compositional maximum to develop. The smaller β_{22}, the closer to unity β_{21} may be and still produce a maximum.

Since $\gamma'_1(0)$ and $\gamma'_2(0)$ are both negative between the plate and compositional minimum (e.g. the curve in Fig. 2 for $\beta_{21} = -1$), the requirement for uphill diffusion may be rearranged as

$$\beta_{21} < -\beta_{22}\left|\frac{\gamma'_2}{\gamma'_1}\right|.$$

Both quantities on the right-hand side are positive; consequently $\beta_{21} < 0$ is a necessary but not sufficient condition for uphill diffusion. $|\beta_{21}|$ must also be larger than approximately $(1/10)\beta_{22}$. The mass flux is still positive in a zone next to the plate if the cross-coupling is this weak. As the magnitude of β_{21} increases, the plane of no flux moves toward the plate. Only for $|\beta_{21}| > \beta_{22}$ can j_2 be negative at the plate.

The velocity at $\eta = \infty$ varies directly with β_{21} (Fig. 3(a)). The increased concentration of component 2 when $\beta_{21} > 0$ causes larger buoyancy forces and greater velocities. In contrast, $\beta_{21} < 0$ decreases γ_2 in the boundary layer which diminishes the buoyancy forces. Hence, $f'(\infty)$ is smaller. It is important to note that where $\gamma_2 < 0$, the buoyancy force generated by component 2 is directed opposite the buoyancy force of component 1. Opposed buoyancy forces are generated even though α_1 and α_2 have the same sign, in contradistinction to the study of Nilson and Baer [12] in which opposed buoyancy forces are created by assigning α_1 and α_2 opposite signs. For Γ greater than some critical value, the velocity at $\eta = \infty$ will be zero marking the limit of unidirectional flow (Fig. 3(a)). This is also the limit of applicability for the stretching transformation and the equations

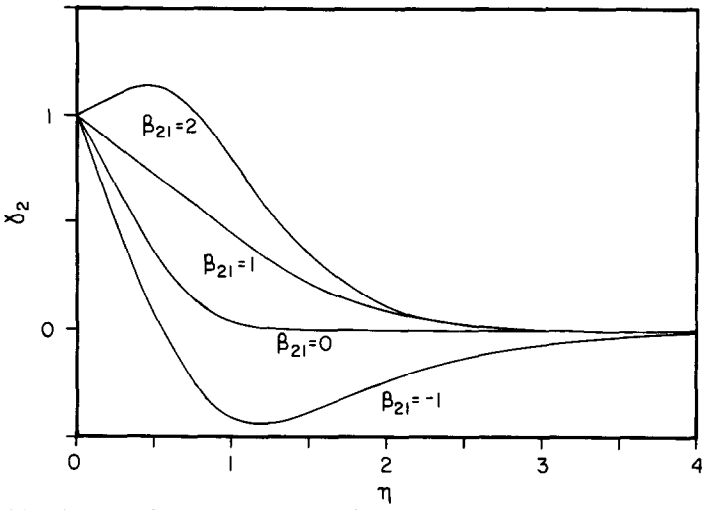

FIG. 2. Compositional profiles for component 2 as a function of β_{21}. $B_1 = B_2 = \beta_{12} = 0$, $\beta_{22} = 10^{-1}$ and $\Gamma = 0.75$ for all curves

as written [12]. We are currently exploring the boundary between upflow and counterflow for these equations.

The relationship of diffusive cross-coupling to boundary layer thicknesses is also fairly simple (Fig. 3(b)). The most striking feature of this diagram is that δ_2 is only a function of β_{21} when $\beta_{22} < \beta_{21}$. In general cross-coupling causes δ_2 to increase with respect to the uncoupled solution. The only exception is when β_{21} is negative and smaller in magnitude than β_{22}.

When $\beta_{22} \ll \beta_{21}$ we find that the proper mass transfer correlation for component 2 is

$$Sh_2 = 0.670[Gr_L Sc(1+\sqrt{(\beta_{22})}\Gamma)(1+\beta_{21}\Gamma)]^{1/4}\beta_{21}/\beta_{22}$$

which corresponds to the linear portion of the curves in Fig. 4(a). When $\beta_{22} \geqslant |\beta_{21}|$ the Sh_2 vs β_{22} curve coincides with or closely parallels that for the uncoupled equations.

Again very interesting behavior results when β_{21} is negative. Recall that the condition for a compositional minimum is a negative mass flux in at least part of the boundary layer. In Fig. 4(b) we plot Sh_2 vs β_{22} for $\beta_{21} = -1$, -0.2 and -0.02. Each curve consists of two pieces divided by a vertical asymptote where

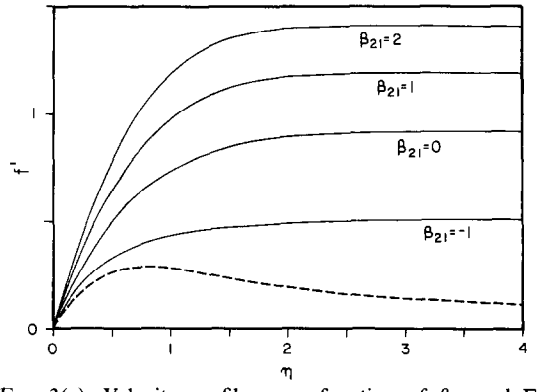

FIG. 3(a). Velocity profiles as a function of β_{21} and Γ. $B_1 = B_2 = \beta_{12} = 0$, $\beta_{22} = 10^{-1}$ and $\Gamma = 0.75$ for all solid curves. Dashed curve shows the effect of increasing the buoyancy ratio when β_{21} is negative: $B_1 = B_2 = \beta_{12} = 0$, $\beta_{21} = -1$, $\beta_{22} = 10^{-1}$ and $\Gamma = 1.05$. Counterflow occurs at approximately $\Gamma = 1.1$.

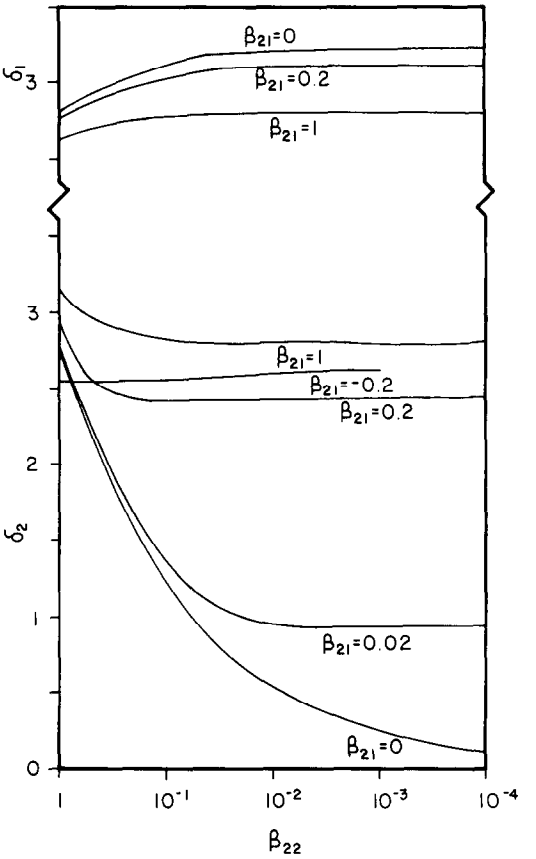

FIG. 3(b). Boundary layer thicknesses as a function of β_{21} and β_{22}. $B_1 = B_2 = \beta_{12} = 0$ and $\Gamma = 0.75$ for all curves. The upper scale is for component 1 while the lower is for component 2.

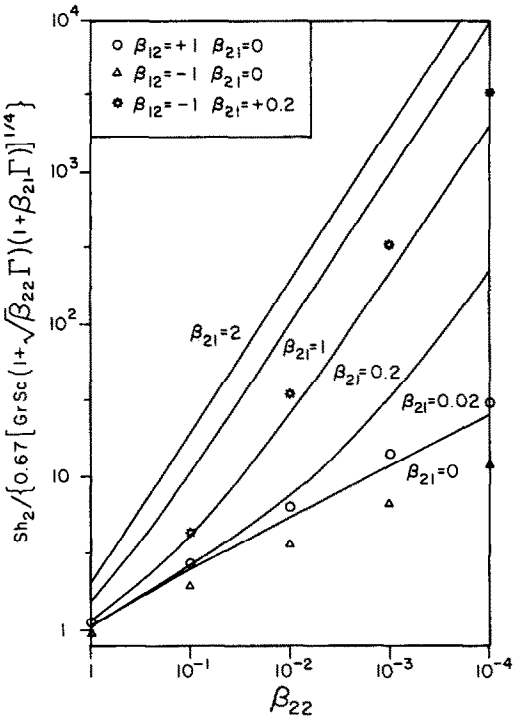

FIG. 4(a). Sh_2 as a function of β_{22} for $\beta_{21} > 0$. $B_1 = B_2 = 0$ and $\Gamma = 0.75$ for all curves. $\beta_{12} = 0$ for all solid lines.

$Sh_2 = 0$. Between $\beta_{22} = 1$ and the vertical asymptote Sh_2 is positive. At first these curves follow the $\beta_{21} = 0$ trend (cf. Fig. 4(a)), but decrease rapidly as the cross-coupling becomes strong enough to create a region of negative mass flux. For β_{22} smaller than the vertical asymptote Sh_2 is negative (i.e. mass transfer from the fluid to the plate). The appropriate correlation in the linear part of the Sh_2 vs β_{22} curve is identical to that given above.

Component 1 is only weakly dependent on β_{21}, but this is only really evident from the boundary layer thickness (Fig. 3(b)). Note that the magnitude of variation in δ_1 with β_{21} is quite small compared to the variation in δ_2, particularly when $\beta_{22} \ll 1$. Unlike δ_2, the relationship between δ_1 and β_{22} is unaffected and δ_1 decreases for β_{21} positive. Sh_1 changes by less than 20% over the range of β_{21} studied (Fig. 6(b)).

Next, we set $\beta_{21} = 0$ in order to examine the flow's response to β_{12}. Compositional profiles for component 1, presented in Fig. 5 for a range of β_{12} values, closely resemble the γ_2 profiles in Fig. 2. Again solution of the uncoupled equations ($\beta_{12} = 0$) is a concave up curve with a maximum at $\eta = 0$ and a minimum at $\eta = \delta_1$; however, extrema may occur in the middle of the boundary layer when $\beta_{12} \neq 0$. The condition for uphill diffusion of component 1 is

$$j_1\gamma_1' = (\gamma_1' + \beta_{12}\gamma_2')\gamma_1' > 0$$

and β_{12} must be nonzero to satisfy this condition. Interestingly enough, the conditions for maxima and minima are the reverse of those for component 2. It is sufficient for β_{12} to be large compared with β_{22} in order to produce a compositional maximum. For instance, $\beta_{12} = 0.5$ and $\beta_{22} = 10^{-2}$ are one such set of parameters. The critical value of β_{12} approaches zero as β_{22} becomes very small. Compositional minima may result when $\beta_{12} < 0$ yet $\beta_{12} < -1$ is required for j_{1w} to be negative.

The relationship between β_{12} and $f'(\infty)$ is quite similar to that discussed above for β_{21}. Although velocities differ in magnitude somewhat the trend shown in Fig. 3(a) is the same for β_{12}. Opposed buoyancy forces due to component 1 arise when the value of β_{12} is in the correct range to produce a compositional minimum. As Γ approaches zero the dominant buoyancy force is due to component 1 and counterflow may result.

Note that Sh_2 (Fig. 4(a)) and δ_2 (Fig. 6(a)) differ

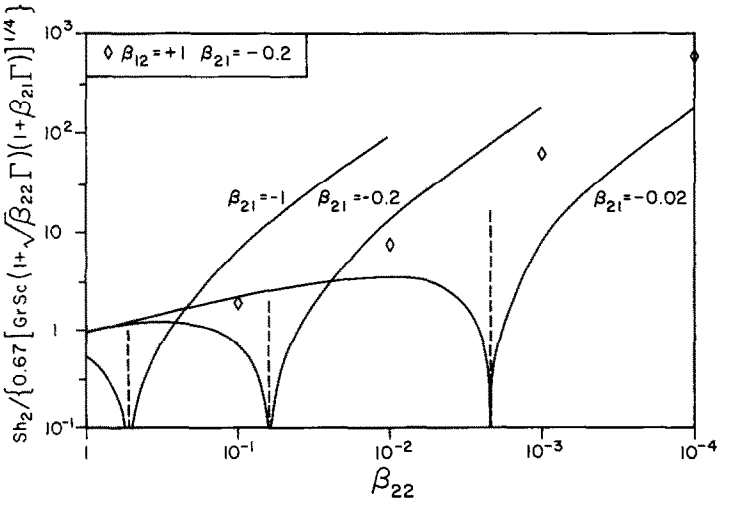

FIG. 4(b). Sh_2 as a function of β_{22} for $\beta_{21} < 0$. For each curve Sh_2 goes to zero at the vertical dashed line. The Sherwood number is negative for β_{22} smaller than this value. Solid lines terminate near the upflow–counterflow boundary. $B_1 = B_2 = 0$ and $\Gamma = 0.75$ for all curves; in addition, $\beta_{12} = 0$ for the solid lines.

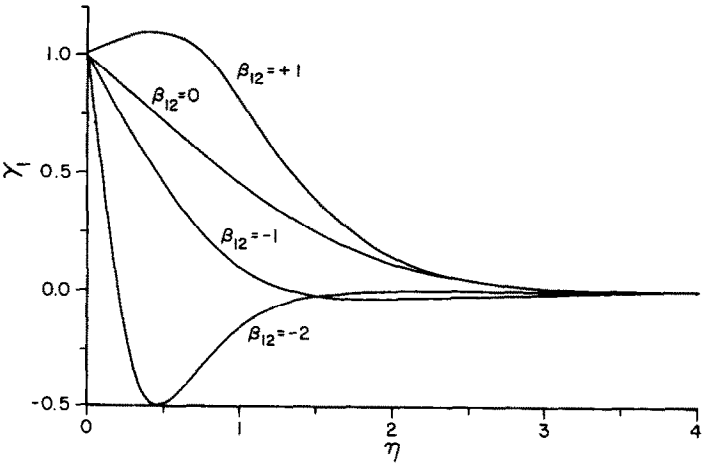

FIG. 5. Compositional profiles for component 1 as a function of β_{12}. $B_1 = B_2 = \beta_{21} = 0$, $\beta_{22} = 10^{-1}$ and $\Gamma = 0.75$ for all curves.

from the uncoupled solution by less than 50% over the range of β_{12} in this study hence $\gamma_2' \sim \delta_2^{-1}$. As β_{22} goes to zero, the cross-coupling contribution to the mass flux, which is proportional to γ_2', increases. If β_{12} is negative, the two components of mass flux must balance in such a way to keep Sh_1 positive. In fact $\delta_1 \sim \delta_2/|\beta_{12}|$ and $Sh_1 \to 0$ for $\beta_{22} \ll 1$. For example, $\delta_1 = \delta_2$ when $\beta_{12} = -1$ (Fig. 6(a)). In contrast, Sh_1 is nearly constant for all β_{22} when $\beta_{12} > 0$ (Fig. 6(b)). The large cross-coupling component of j_1 is offset by the compositional maximum which increases in magnitude as $\beta_{22} \to 0$. δ_1 does not participate in this balance and remains constant.

Finally, we consider the effects of two off-diagonal diffusivities. It is instructive to consider the limitations imposed by thermodynamic constraints (6). Since there is a reciprocal relationship between the off-diagonal terms

$$(-\tfrac{1}{4}\beta_{22}^2 + \tfrac{1}{2}\beta_{22} - \tfrac{1}{4}) < \beta_{12}\beta_{21} < \beta_{22}$$

if one is very large compared to these bounds, the other must be very small. Both cross terms can be

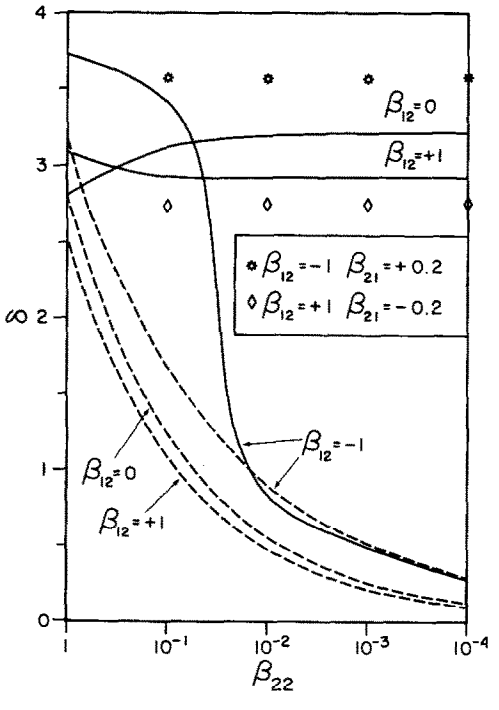

FIG. 6(a). Boundary layer thicknesses as a function of β_{12} and β_{22}. $B_1 = B_2 = 0$ and $\Gamma = 0.75$ for all curves, and $\beta_{21} = 0$ except for the open symbols. Dashed lines are for δ_2; solid lines and open symbols are for δ_1. Recall that when both off-diagonal terms are nonzero the thermodynamics restrict the range of β_{22} over which solutions are possible.

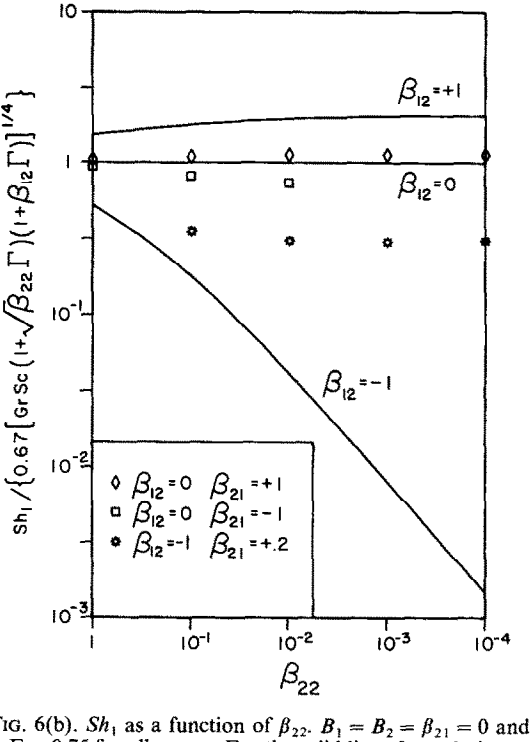

FIG. 6(b). Sh_1 as a function of β_{22}. $B_1 = B_2 = \beta_{21} = 0$ and $\Gamma = 0.75$ for all curves. For the solid lines $\beta_{21} = 0$ also.

order one only when both are the same sign and when β_{22} is order one.

Perhaps the most interesting question is whether both components can display compositional extrema at the same time? We have found that the two components cannot both have maxima or both have minima. This is quite easily shown for maxima as long as the restrictions for a single off-diagonal term are still valid. Recall that $\beta_{21} > 1$ and $\beta_{12} > \beta_{22}$ are the appropriate conditions; however, this implies that $\beta_{12}\beta_{21} > \beta_{22}$ if both conditions are met. This violates thermodynamic condition (6b). Similarly, the requirements for Sh_1 and Sh_2 negative are $\beta_{12} < -1$ and $\beta_{21} < -\beta_{22}$, respectively. Again combination of these violates the thermodynamic constraints. Although this appears to allow compositional minima as long as $Sh_1 > 0$ and $Sh_2 > 0$, our work shows that this does not happen. Apparently the presence of both off-diagonal terms in the diffusivity matrix further restricts the occurrence of compositional extrema.

In contrast, one component can have a maximum while the other component has a minimum. The Sherwood number for the component with the minimum must be positive, since both contributions to the mass flux for that component are positive. For example, $\beta_{21} < 0$ is required to produce a minimum in the compositional profile for component 2 while a maximum in the component 1 composition profile implies $\gamma_1'(0) > 0$. Consequently, both terms in the component 2 mass flux

$$j_{2w} = -\beta_{21}\gamma_1'(0) - \beta_{22}\gamma_2'(0)$$

are positive at the plate.

The combination of one negative cross term and one positive cross term produces the most significant changes in Sherwood number and boundary layer thickness. Figure 4(b) shows that Sh_2 remains positive for small β_{22} if $\beta_{12} = 1$ when $\beta_{21} = -0.2$. Similarly Sh_1 becomes independent of β_{22} when $\beta_{12} = -1$ if $\beta_{21} = 0.2$ (Fig. 6(b)).

These results must be applied with care because the scaled weight fractions lie outside the normal range, $0 \leqslant \gamma_i \leqslant 1$, for certain combinations of parameters. This happens whenever a compositional maximum or minimum develops. As a result the actual weight fractions could be unphysical ($\bar{\omega}_i < 0$ or $\bar{\omega}_1 > 1$) in parts of the boundary layer. Indeed, Gupta and Cooper [25] argue that the diffusivity matrix must be composition dependent to prevent this.

Variable viscosity

Although we have comparatively few variable viscosity results, they are sufficient to demonstrate general trends. This topic is most easily understood by considering the physics of the boundary layer. Since the stretching transformation removed inertial forces, equation (4′) represents a balance between viscous forces opposing the flow and buoyancy forces driving the flow. Viscous forces depend on the boundary layer's viscosity structure and may be substantially altered if viscosity is a function of composition. Compensating adjustments in buoyancy are accommodated principally through changes in boundary layer thickness.

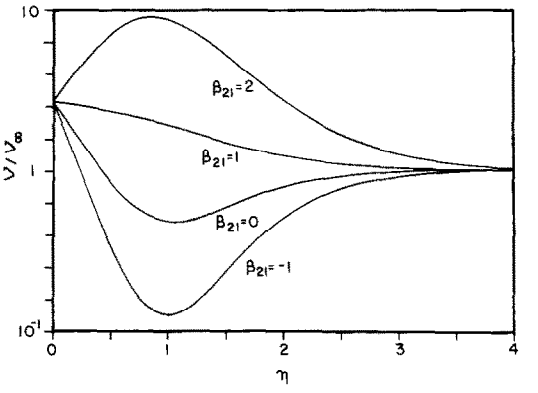

FIG. 7(a). Viscosity profile as a function of β_{21}. $B_1 = -2.0$, $B_2 = 3.0$, $\beta_{12} = 0$, $\beta_{22} = 10^{-1}$ and $\Gamma = 0.75$ for all curves

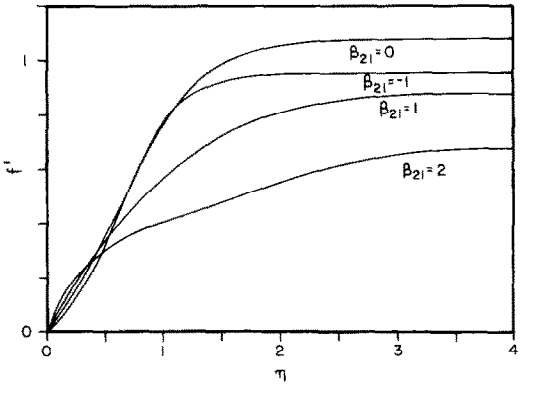

FIG. 7(b). Velocity profiles as a function of β_{21} with composition-dependent viscosity. $B_1 = -2.0$, $B_2 = 3.0$, $\beta_{12} = 0$, $\beta_{22} = 10^{-1}$ and $\Gamma = 0.75$ for all curves.

Figures 7(a) and (b) show viscosity and velocity profiles for several combinations of B_1, B_2 and β_{21}. These may be separated into three groups.

(1) $\nu \geqslant \nu_\infty$ everywhere in the boundary layer. Velocities are smaller and boundary layer thicknesses are greater than the corresponding isoviscous flow.

(2) $\nu \leqslant \nu_\infty$ everywhere in the boundary layer. Velocities are larger and boundary layer thicknesses are smaller than the corresponding isoviscous flow.

(3) $\nu \geqslant \nu_\infty$ in part of the boundary layer and $\nu \leqslant \nu_\infty$ in the rest of the boundary layer. Adjustments in the force balance are much more complicated in this case.

All parameters of the model play a role in determining the viscosity structure. This means that an arbitrary viscosity structure cannot be imposed on the flow merely by choice of B_1 and B_2. The quantity $B_1 + B_2$, however, defines ν_w since the constant concentration boundary condition is applied there. If $B_1 + B_2 > 0$ then $\nu_w > \nu_\infty$, and if $B_1 + B_2 < 0$ then $\nu_w < \nu_\infty$. The viscosity far away from the wall will then

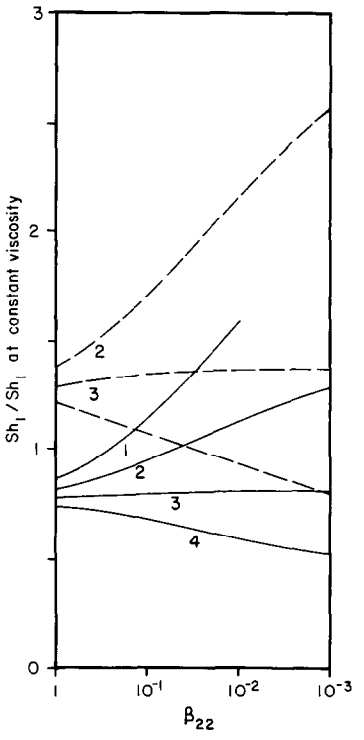

FIG. 8(a). Ratio of Sh_1 with variable viscosity to Sh_1 with constant viscosity as a function of β_{21} and β_{22}. $\beta_{12} = 0$ and $\Gamma = 0.75$ for all curves. (a) $\beta_{21} = -1$; (2) $\beta_{21} = 0$; (3) $\beta_{21} = 1$; (4) $\beta_{21} = 2$. Solid lines denote $B_1 = -2$ and $B_2 = 3$. Dashed lines denote $B_1 = -5.5$ and $B_2 = 3.7$.

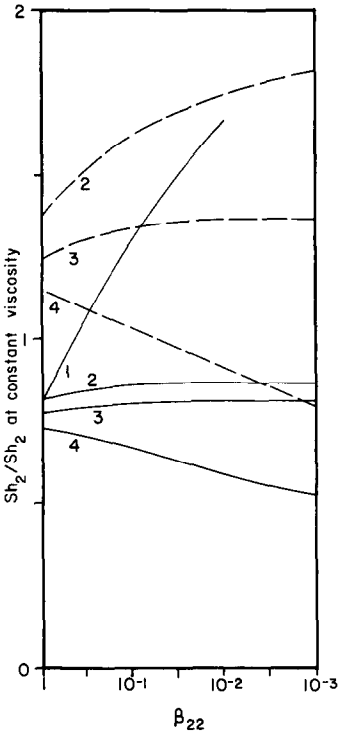

FIG. 8(b). Ratio of Sh_2 with variable viscosity to Sh_2 with constant viscosity as a function of β_{21} and β_{22}. $\beta_{12} = 0$ and $\Gamma = 0.75$ for all curves. (1) $\beta_{21} = -1$; (2) $\beta_{21} = 0$; (3) $\beta_{21} = 1$; (4) $\beta_{21} = 2$. Solid lines denote $B_1 = -2$ and $B_2 = 3$. Dashed lines denote $B_1 = -5.5$ and $B_2 = 3.7$.

depend on the sign and magnitude of all parameters.

We have considered two cases: (1) $B_1 = -2$ and $B_2 = 3$; (2) $B_1 = -5.5$ and $B_2 = 3.7$. We have used the method of Shaw [22] to calculate viscosities for silicate liquids with compositions corresponding to the desired wall and infinity values. Then we fit an exponential function, equation (2), to these viscosities. The first set of values correspond to a low SiO_2, low H_2O magma (basaltic) while the second set correspond to a high SiO_2, high H_2O magma (rhyolitic). Although B_1 and B_2 have the same sign for both, $v_w > v_\infty$ in the first case and $v_w < v_\infty$ in the second case.

A convenient measure of the change due to composition-dependent viscosity is the ratio of Sh_1 for the variable viscosity case to Sh_1 for the isoviscous case with all other parameters the same (Figs. 8(a) and (b)). When this ratio is greater than unity, variable viscosity caused steeper concentration gradients and increased mass fluxes. The reverse is true for a ratio less than unity. Sh_i changes by less than a factor of three while the viscosity may vary by more than an order of magnitude (Fig. 7(a)). Variation in Sh appears to be proportional to the magnitude of $B_1 + B_2$.

The products $B_1^* = B_1\beta_{12}$ and $B_2^* = B_2\beta_{21}$ are useful for showing changes in velocity (Fig. 7(b)). The sign of B_i^* determines the effect on the flow of component i. The cross terms determine which component(s) are enriched or depleted in the boundary layer compared to the uncoupled equations. The sign of B_i determines whether the change in concentration increases or decreases the viscosity. Positive B_i^* means that component i will contribute to decreased velocities. When negative that component will contribute toward increased velocities. Of course concentration changes affect buoyancy forces as well, particularly when compositional extrema are present, and may be more important than the viscosity changes.

Effective binary diffusion coefficients

For systems with three or more chemical components, measurements of EBDCs are much more common in the literature than phenomenological coefficients discussed above. EBDCs are the only data currently available for magmas, for example. Since experimental data necessary for calculating the β_{ij} are generally unavailable, can EBDCs be used to approximate the full phenomenological formulation?

If one assumes the diffusion coefficients are not functions of composition, setting $\beta_{12} = \beta_{21} = 0$ yields the pseudo-binary equations which have already been discussed. β_{22}, now defined as the ratio of reference EBDCs ($D_{2\infty}/D_{1\infty}$), is the only parameter that can be adjusted to create the best approximation to the full phenomenological formulation. This method, utilized in ref. [19] for example, fails for two reasons. First,

the pseudo-binary equations contain an inverse relationship between δ_2 and Sh_2 while phenomenological cross-coupling produces increases in both these quantities (Figs. 3(b) and 4(a)). For K_2O–SrO–SiO_2 [28] the pseudo-binary β_{22} is equal to 0.7 which predicts $\delta_2 = 2.6$ and $Sh_2/[Gr_L Sc]^{1/4} = 0.85$. The phenomenological solution is $\delta_2 = 2.23$ and $Sh_2/[Gr_L Sc]^{1/4} = -245$. The boundary layer thickness is reasonably approximated, but the magnitude and sign of Sh_2 are seriously in error. A system such as NaCl–$MgCl_2$–H_2O would be better approximated since the phenomenological β_{22} is close to unity. Second, constant EBDCs cannot produce compositional extrema. This point has been discussed more fully above.

In general EBDCs will be functions of $\bar{\omega}_1$ and $\bar{\omega}_2$. Delaney and Karsten [29] found that the effective binary diffusion coefficient of H_2O in rhyolite melt is an exponential function of the H_2O concentration. EBDCs for SiO_2 have been measured in anhydrous melts ranging in composition from basalt to rhyolite [30, 31]. We have fit these data to an exponential function as well. Conservation equations for this functional dependence are included in the Appendix.

Although we do not have phenomenological coefficients necessary for a quantitative comparison, a few qualitative remarks are in order. The trend of δ_i vs β_{22} for composition dependent EBDCs (Fig. 9) is essentially parallel to that for constant diffusivities. As β_{22} becomes very small, composition dependence is comparatively unimportant, so all the curves converge. We have not shown a plot of Sh_2 because these trends also parallel the constant diffusivity solution. As a result, this form of composition dependence does not eliminate the problem of matching both δ_2 and Sh_2. Several composition profiles are plotted in Fig. 10. A component is either enriched or depleted in the boundary layer according to the sign of D_i. These profiles are similar to those in Figs. 2(a) and 5 except that compositional extrema are not possible.

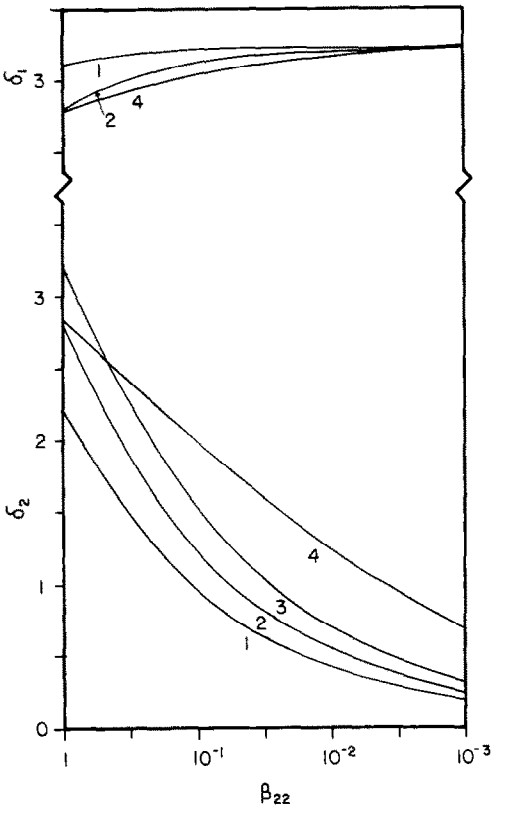

FIG. 9. Boundary layer thicknesses as a function of β_{22} for composition-dependent EBDCs. $B_1 = B_2 = A_{12} = 0$ and $\Gamma = 0.75$ for all curves. (1) $A_{11} = 2$, $A_{21} = 0$, $A_{22} = -1.5$; (2) $A_{11} = A_{21} = A_{22} = 0$; (3) $A_{11} = -2$, $A_{21} = 0$, $A_{22} = 1.5$; (4) $A_{11} = 2$, $A_{21} = 4$, $A_{22} = -1.5$. The upper scale is for component 1 while the lower is for component 2.

CONCLUSIONS

We have numerically simulated boundary layer flow in an isothermal ternary fluid driven by compositionally induced buoyancy. The diffusive fluxes were modeled using phenomenological theory. Some attention was given to the affect of composition-dependent Newtonian viscosity. The major conclusions of this study are summarized below.

(1) The flow's behavior is governed by the sign and magnitude of each element in the phenomenological diffusivity matrix

$$\begin{bmatrix} 1 & \beta_{12} \\ \beta_{21} & \beta_{22} \end{bmatrix}.$$

The off-diagonal elements, β_{12} and β_{21}, are responsible for diffusive cross-coupling. The size of the off-diagonal elements compared to the on-diagonal matrix elements $(1, \beta_{22})$ determines whether or not the cross-coupling significantly changes the boundary layers' characteristics. β_{22} must be at least an order of magnitude larger than the absolute value of an off-diagonal element in order to neglect that term. The following statements apply when one or both off-diagonal elements are significant.

(2) $f'(\infty)$ is positively correlated with β_{12} and β_{21}. When β_{12} and/or β_{21} are negative, counterflow is possible for certain values of Γ.

(3) Very strong cross-coupling is characterized by the formation of compositional extrema in the boundary layers' interior. A maximum for component i may occur when the off-diagonal term in the ith row is sufficiently large compared to the on-diagonal term in the same column. A minimum for component i may occur when the off-diagonal term in the ith row is negative. Around the extremum one or more components lie outside the usual compositional range, $0 < \gamma_i < 1$. The components cannot both exhibit maxima or both minima, although one may have a maximum while the other has a minimum.

(4) If $|\beta_{21}| \geqslant \beta_{22}$, Sh_2 is proportional to β_{21}/β_{22}. Sh_i may be negative when the off-diagonal term in the ith row is negative and sufficiently large in absolute value

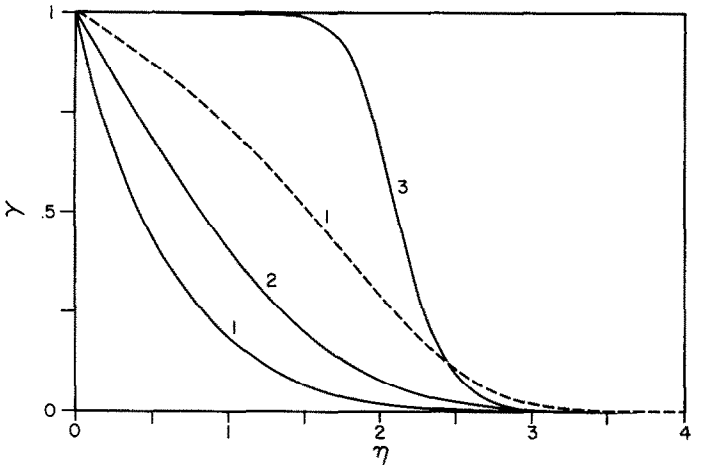

FIG. 10. Compositional profiles using composition-dependent EBDCs. $B_1 = B_2 = 0$, $\beta_{22} = 1$ and $\Gamma = 0.75$ for all curves. The dashed line is for component 1 and solid lines are for component 2. (1) $A_{11} = -2.0$, $A_{12} = A_{21} = 0$ and $A_{22} = -1.5$; (2) $A_{11} = A_{12} = A_{21} = A_{22} = 0$; (3) $A_{11} = 2.0$, $A_{12} = 0$, $A_{21} = 14$ and $A_{22} = -1.5$.

compared to the on-diagonal term in the same row. A negative Sherwood number means that a component is transferred from the fluid to the wall.

(5) Composition-dependent viscosity changes the boundary layer according to whether the viscosity is higher or lower than the ambient fluid. Increased viscosity leads to thicker boundary layers and smaller mass transfer rates and vice versa for a less viscous boundary layer. The sign of B_1, B_2 and $B_1 + B_2$ are important parameters determining the viscosity profile.

(6) Effective binary diffusion coefficients, even when functions of composition, do not admit compositional extrema. As such this approach cannot be used to approximate a ternary flow, and, by analogy, any multicomponent system with large off-diagonal elements.

(7) Failure to properly account for diffusive coupling in multicomponent flows can lead to invalid deductions for many systems of interest to geochemists, geologists and ceramic scientists, including boundary layer flows in large crustal magma reservoirs.

Acknowledgements—This research ws supported by an NSF graduate fellowship to AFT and by NSF EAR85-19900 and NSF EAR86-08284 to FJS. Numerical calculations were supported by the Princeton University Computer Center and the Office of the Provost of the University of California at Santa Barbara. We thank an anonymous reviewer for many helpful suggestions. We are also indebted to Ellie Dzuro for preparing the manuscript and to Dave Crouch and Heather Sloan for preparing the figures.

REFERENCES

1. A. Bejan, *Convective Heat Transfer*. Wiley, New York (1984).
2. Y. Jaluria, *Natural Convection Heat and Mass Transfer*. Pergamon Press, Oxford (1980).
3. H. K. Kuiken, An asymptotic solution for large Prandtl number free convection, *J. Engng Math.* **2**, 355–371 (1968).
4. G. W. Morgan and W. H. Warner, On heat transfer in laminar boundary layers at high Prandtl number, *J. Aeronaut. Sci.* **23**, 937–948 (1956).
5. K. Stewartson and L. T. Jones, The heated vertical plate at high Prandtl number, *J. Aeronaut. Sci.* **24**, 379–380 (1957).
6. E. M. Sparrow and J. L. Gregg, Similar solutions for free convection from a nonisothermal vertical plate, *Trans. ASME* **80**, 379–386 (1958).
7. J. R. Lloyd, E. M. Sparrow and E. R. G. Eckert, Laminar, transition and turbulent natural convection adjacent to inclined and vertical surfaces, *Int. J. Heat Mass Transfer* **15**, 457–473 (1972).
8. D. V. Kemp, Marginal upflow in magma chambers: an evaluation of boundary layer convection induced by chemical buoyancy, unpublished senior thesis, Princeton University, Princeton, New Jersey (1984).
9. W. G. Mathers, A. J. Madden, Jr. and E. L. Piret, Simultaneous heat and mass transfer in free convection, *Ind. Engng Chem.* **49**, 961–968 (1957).
10. E. V. Somers, Theoretical considerations of combined thermal and mass transfer from a vertical flat plate, *J. Appl. Mech.* **23**, 295–301 (1956).
11. D. A. Saville and S. W. Churchill, Simultaneous heat and mass transfer in free convection boundary layers, *A.I.Ch.E. Jl* **16**, 268–273 (1970).
12. R. H. Nilson and M. R. Baer, Double-diffusive counterbuoyant boundary layer in laminar natural convection, *Int. J. Heat Mass Transfer* **25**, 285–287 (1982).
13. E. M. Sparrow, W. J. Minkowycz and E. K. G. Eckert, Transpiration-induced buoyancy and thermal diffusion–diffusion thermo in a helium–air free convection boundary layer, *J. Heat Transfer* **86**, 508–514 (1964).
14. E. L. Cussler, *Multicomponent Diffusion*, pp. 66–68. Elsevier, Amsterdam (1976).
15. H. Sugawara, K. Nagata and K. S. Goto, Interdiffusivities matrix of CaO–Al_2O_3–SiO_2 melt at 1723 K to 1823 K, *Metall. Trans.* **8B**, 605–612 (1977).
16. A. K. Varshneya and A. R. Cooper, Diffusion in the system K_2O–SrO–SiO_2: III. Interdiffusion coefficients, *J. Am. Ceram. Soc.* **55**, 312–317 (1972).
17. D. G. Miller, A. W. Ting, J. A. Rard and L. B. Eppstein, Ternary diffusion coefficients of the brine systems NaCl (0.5 M)–Na_2SO_4 (0.5 M)–H_2O and NaCl (0.489 M)–

$MgCl_2$ (0.051 M)–H_2O (seawater composition) at 25°C, *Geochim. Cosmochim. Acta* **50,** 2397–2403 (1986).
18. H. R. Shaw, Diffusion of H_2O in granitic liquids: part I. Experimental data: part II. Mass transfer in magma chambers. In *Geochemical Transport and Kinetics* (Edited by A. W. Hoffman), pp. 139–170. Carnegie Institute (1974).
19. A. R. McBirney, B. H. Baker and R. H. Nilson, Liquid fractionation. Part I: basic principles and experimental simulations, *J. Volcanol. Geotherm. Res.* **24,** 1–24 (1985).
20. T. F. Soules, Molecular dynamic calculations of glass structure and diffusion in glass, *J. Non-Crystall. Solids* **49,** 29–52 (1982).
21. F. J. Spera, D. A. Yuen and S. J. Kirschvink, Thermal boundary layer convection in silicic magma chambers: effects of temperature dependent rheology and implications for thermogravitational chemical fractionation, *J. Geophys. Res.* **87,** 8755–8767 (1982).
22. H. R. Shaw, Viscosities of magmatic silicate liquids: an empirical method of prediction, *Am. J. Sci.* **272,** 870–893 (1972).
23. Y. Bottinga and D. F. Weill, Densities of liquid silicate systems calculated from partial molar volumes of oxide components, *Am. J. Sci.* **269,** 169–182 (1970).
24. Y. Bottinga and D. F. Weill, The viscosity of magmatic silicate liquids: a model for calculation, *Am. J. Sci.* **272,** 438–475 (1972).
25. P. K. Gupta and A. R. Cooper, Jr., The [D] matrix for multicomponent diffusion, *Physica* **54,** 39–59 (1971).
26. A. Acrivos, The asymptotic form of the laminar boundary-layer mass-transfer rate for large interfacial velocities, *J. Fluid Mech.* **12,** 337–357 (1962).
27. F. J. Spera, D. A. Yuen and D. V. Kemp, Mass transfer rates along vertical walls in magma chambers and marginal upwelling, *Nature* **310,** 764–767 (1984).
28. A. R. Cooper and A. K. Varshneya, Diffusion in the system K_2O–SrO–SiO_2: I. Effective binary diffusion coefficients, *J. Am. Ceram. Soc.* **51,** 103–106 (1968).
29. J. R. Delaney and J. L. Karsten, Ion microprobe studies of water in silicate melts: concentration-dependent water diffusion in obsidian, *Earth Planet. Sci. Lett.* **52,** 191–202 (1981).
30. E. B. Watson, Basalt contamination by continental crust: some experiments and models, *Contrib. Mineral. Petrol.* **80,** 73–87 (1982).
31. C. E. Lesher and D. Walker, Solution properties of silicate liquids from thermal diffusion experiments, *Geochim. Cosmochim. Acta* **50,** 1397–1411 (1986).
32. S. Clark, F. J. Spera and D. A. Yuen, Steady state double-diffusive convection in magma chambers heated from below. In *Magmatic Processes: Physicochemical Principles* (Edited by B. O. Mysen), pp. 289–305. The Geochemical Society (1987).

APPENDIX

We have chosen an exponential function similar to equation (2) for the dependence of diffusivities on composition

$$D_1 = D_{1\infty} \exp [A_{11}\omega_1 + A_{12}\omega_2] \quad \text{(A1a)}$$

$$D_2 = D_{2\infty} \exp [A_{21}\omega_1 + A_{22}\omega_2]. \quad \text{(A1b)}$$

Now the fluxes given by equation (5) are rewritten using equations (A1)

$$j_1 = -\exp [A_{11}\omega_1 + A_{12}\omega_2]\nabla\omega_1 \quad \text{(A2a)}$$

$$j_2 = -\beta \exp [A_{21}\omega_1 + A_{22}\omega_2]\nabla\omega_2. \quad \text{(A2b)}$$

Conservation equations given in equations (7) become

$$u\frac{\partial\omega_1}{\partial x} + v\frac{\partial\omega_1}{\partial y} = \frac{1}{Sc}\left\{\frac{\partial^2\omega_1}{\partial y^2} + A_{11}\left(\frac{\partial\omega_1}{\partial y}\right)^2 + A_{12}\frac{\partial\omega_1}{\partial y}\frac{\partial\omega_2}{\partial y}\right\} \times \exp [A_{11}\omega_1 + A_{12}\omega_2] \quad \text{(A3a)}$$

$$u\frac{\partial\omega_2}{\partial x} + v\frac{\partial\omega_2}{\partial y} = \frac{1}{Sc}\beta\left\{\frac{\partial^2\omega_2}{\partial y^2} + A_{21}\frac{\partial\omega_1}{\partial y}\frac{\partial\omega_2}{\partial y} + A_{22}\left(\frac{\partial\omega_2}{\partial y}\right)^2\right\} \times \exp [A_{21}\omega_1 + A_2\omega_2]. \quad \text{(A3b)}$$

Finally, introduction of the stretching transformation into equations (A3) and setting $Sc = \infty$ yields the set of equations to be used in place of equations (7)

$$[\gamma_1'' + A_{11}(\gamma_1')^2 + A_{12}\gamma_1'\gamma_2']\exp [A_{11}\gamma_1 + A_{12}\gamma_2] + f\gamma_1' = 0 \quad \text{(A4a)}$$

$$\beta_{22}\{\gamma_2'' + A_{21}\gamma_1'\gamma_2' + A_{22}(\gamma_2')^2\}\exp [A_{21}\gamma_1 + A_{22}\gamma_2] + f\gamma_2' = 0. \quad \text{(A4b)}$$

We retain the definition of Sh given in equations (10) with D_{ii} replaced by D_i. Inserting the mass flux from equations (A2) and integrating leads to the composition dependent EBDC expression for Sh_i

$$Sh_1 = -1.2408(Gr_L Sc)^{1/4} \cdot [\gamma_1'(0)\exp (A_{11} + A_{12})] \quad \text{(A5a)}$$

$$Sh_2 = -1.2408(Gr_L Sc)^{1/4} \cdot [\gamma_2'(0)\exp (A_{21} + A_{22})]. \quad \text{(A5b)}$$

ECOULEMENT DE CONVECTION NATURELLE AVEC COUCHE LIMITE DANS DES SYSTEMES TERNAIRES ISOTHERMES : ROLE DU COUPLAGE DIFFUSIF

Résumé—On étudie les effets de couplage croisé diffusif sur une couche limite de convection naturelle isotherme dans un fluide à grand *Sc*. Les résultats montrent que le coefficient de diffusion hors-diagonale est important lorsque le rapport approprié β_{12}/β_{22} ou β_{21}/β_{22} est supérieur à 10^{-1} environ. Une diffusion et des extremas de composition résultants peuvent résulter de $\beta_{12} > \beta_{22}$ ou $\beta_{12} < 0$ pour le composant 1 et de $\beta_{21} > 1$ ou $\beta_{21} < 0$ pour le composant 2. Un contrecourant peut résulter de $\beta_{21} < 0$ ou $\beta_{12} < 0$ même pour des rapports positifs de flottement. Des coefficients de diffusion binaire effective ne conviennent pas pour représenter des systèmes multicomposants avec des grands coefficients de diffusion hors-diagonale. Des déterminations publiées de matrice de diffusion pour différents systèmes multicomposants, en négligeant les contributions hors-diagonale aux flux chimiques, peuvent conduire à de fortes erreurs sur les flux de masse transférés dans des cas de systèmes géochimiques et industriels importants.

GRENZSCHICHTSTRÖMUNGEN BEI NATÜRLICHER KONVEKTION IN ISOTHERMEN TERNÄREN GEMISCHEN—EINFLUSS DER ANKOPPLUNG DURCH DIFFUSION

Zusammenfassung—Die Auswirkungen der diffusiven Querkopplung auf eine isotherme Grenzschicht bei natürlicher Konvektion in einem Fluid mit großer Schmidt-Zahl wurde untersucht. Die Ergebnisse zeigen, daß das Nebenelement der Diffusionskoeffizientenmatrix dann wichtig ist, wenn das Verhältnis β_{12}/β_{22} oder β_{21}/β_{22} größer als etwa 0,1 ist. Aufwärtsdiffusion und dadurch bedingte Extremwerte in der Zusammensetzung können auftreten, wenn $\beta_{12} > \beta_{22}$ oder $\beta_{12} < 0$ für die Komponente 1 und $\beta_{21} > 1$ oder $\beta_{21} < 0$ für die Komponente 2 ist. Gegenströmung kann auftreten, wenn $\beta_{21} < 0$ oder $\beta_{12} < 0$ ist, selbst beim Vorhandensein von Auftrieb. Effektive binäre Diffusionskoeffizienten sind ungeeignet, um Vielkomponentensysteme mit großen Nebenelementen in der Matrix der Diffusionskoeffizienten zu beschreiben. Veröffentlichungen der gesamten Diffusionsmatrix einiger Vielkomponentensysteme führen zu dem Schluß, daß die Vernachlässigung der Anteile der Nebenelemente am chemischen Strom zu großen Fehlern bei den Stoffströmen in Vielkomponentensystemen führen können, wie sie in Industrie und Geochemie vorkommen.

ЕСТЕСТВЕННОКОНВЕКТИВНЫЕ ТЕЧЕНИЯ В ПОГРАНИЧНЫХ СЛОЯХ ИЗОТЕРМИЧЕСКИХ ТРЕХКОМПОНЕНТНЫХ СИСТЕМ: РОЛЬ ВЗАИМОДИФФУЗИИ

Аннотация—Исследуется влияние взаимодиффузии на изотермический естественноконвективный пограничный слой в жидкости с большим значением числа *Sc*. Результаты показывают, что недиагональный коэффициент диффузии существенен, когда соответствующее отношение β_{12}/β_{22} или β_{21}/β_{22} больше $\sim 10^{-1}$. Диффузия в направлении отрицательного градиента концентрации и сопровождающие композиционные экстремумы могут возникать при $\beta_{12} > \beta_{22}$ или $\beta_{12} < 0$ для компоненты 1 и при $\beta_{21} > 1$ или $\beta_{21} < 0$ для компоненты Д. Встречное течение может возникнуть при $\beta_{21} < 0$ или $\beta_{12} < 0$ даже для положительных отношений подъемных сил. Эффективные коэффициенты бинарной диффузии непригодны для представления многокомпонентных систем с большими недиагональными коэффициентами диффузии. Опубликованные результаты по определению полной диффузионной матрицы нескольких многокомпонентных систем подразумевают, что пренебрежение недиагональными вкладами в химический поток может дать большие погрешности в интенсивностях массопереноса в многокомпонентных системах, имеющих геохимическое и промышленное значение.